Surface Shape Matching and Analysis using Intrinsic Coordinate Parameterizations

Shantanu H. Joshi[1][⋆], Jie Shi[2], Yalin Wang[2], Katherine L. Narr[1,3],
Arthur W. Toga[1], and Roger P. Woods[1,3]

[1] Laboratory of Neuro Imaging, University of California Los Angeles, CA, USA
[2] School of Computer Sci. and Engineering, Arizona State University, Tempe, USA
[3] Department of Psychiatry and Biobehavioral Sciences,
University of California Los Angeles, CA, USA

Abstract. This paper presents a geometric method for parameterization, matching, and analysis of surface shapes. Surfaces are parameterized and represented by intrinsic coordinate maps derived from the conformal structure of the shape. This parameterization is invariant to rigid transformations of the shape, as well as angle-preserving parameterizations of the surface. Shape matching between coordinate maps of two surfaces is achieved by i) deforming the isothermal curves of the intrinsic parameterization under a nonlinear transformation, and ii) locally reparameterizing the isothermal curves to yield invariant diffeomorphic matchings. Experimental results are shown in synthetic data as well as neuroanatomical shapes such as the hippocampus and the cortex.

1   Introduction

Over the past decade, we have seen diverse approaches and applications, both in the continuous and the discrete setting for geometric shape modeling. The different approaches for surface modeling and shape analysis are usually fine tuned for the problem in hand. For computer aided design (CAD) applications, the computer graphics community is interested in parameterized or even parametric surface modeling [1]. The spectral shape approach [2] has been originally proposed for computer vision applications such as 3D shape retrieval and recognition, although it has also been recently applied to anatomical shapes [3–5]. Similarly, Fourier-based modeling approaches such as SPHARM and its variations [6–8] have been proposed for brain subcortical structures. A slightly different approach models the medial information in elongated shapes and represents it using medial representations [9, 10] and its variants, M-reps [11], or continuous M-reps [12]. The LDDMM approach [13] relies on high- (usually infinite) dimensional embeddings of shapes in ambient manifolds and finds an optimal matching between objects through momentum fields. Another interesting recent approach [14] represents and models vector fields on surfaces and considers a

space of such surfaces. A slightly different approach [15] uses distributions or currents for modeling shapes of surfaces. There is also the widely used landmark based approach [16, 17] with a well defined statistical formulation.

It is often useful to directly analyze parameterized representations of surface shapes, where quantities such as magnitudes and directions of deformations have convenient physical interpretations. Thus, parameterization-based approaches to shape surface modeling are still considered beneficial and will continue to be developed. Recently, Auzias et al. [18] proposed a model-based parameterization of the cortical surface, where sulci and gyri are constrained to a specific coordinate system. In our work, we represent surfaces using intrinsic curves and allow a continuous deformation based matching of the surfaces via the curves. Surfaces have been previously approximated by curves (for example, see NURBS [1]) in the field of computer graphics, strictly for the purpose of surface editing and deformations, and more recently for facial recognition and analysis [19].

In this paper, we propose an approach that defines an intrinsic coordinate parameterization on the surface which is defined by the surface conformal structure, and present a novel approach for matching the underlying coordinate mappings across different shapes. This method is general and can be applied to a wide variety of shapes. Our approach directly represents the coordinate system by isothermal curves and deforms the coordinate systems via invariant mappings between them. As shown in this paper, this idea has important implications for analyzing anatomical form. This paper is organized as follows: Sec. 2 introduces the surface shape representation, Sec. 3 outlines a method for elastically matching the coordinate systems across shapes, followed by experimental results (Sec. 4) on synthetic data, hippocampal shapes, and the cortex.

2   Surface Representation via Intrinsic Coordinate Maps

We consider a smooth, two-dimensional, genus zero, oriented surface $\mathcal{S}$, and assume that it admits a smooth parameterization $\mathbf{x} : \mathcal{D} \to \mathbb{R}^3$. The domain $\mathcal{D}$ can either be a unit plane or a sphere $\mathbb{S}^2$, although for the purpose of this paper, we will assume $\mathcal{D} \equiv (u, v) \subset \mathbb{R}^2$. Specifically $\mathcal{D} \equiv [0, 1] \times [0, 1]$. Further we also assume that the parameterization $\mathbf{x}$ is isothermal. This means that the local coordinates of the parameterization admit a conformal mapping from a neighborhood of the surface $\mathcal{S}$ to the Euclidean plane. Then the coordinate curves of the parameterization $\mathbf{x}$ are also isothermal. This condition implies that

$$\langle \frac{\partial \mathbf{x}}{\partial u}, \frac{\partial \mathbf{x}}{\partial u} \rangle = \langle \frac{\partial \mathbf{x}}{\partial v}, \frac{\partial \mathbf{x}}{\partial v} \rangle, \text{ and } \langle \frac{\partial \mathbf{x}}{\partial u}, \frac{\partial \mathbf{x}}{\partial v} \rangle = 0, \tag{1}$$

thus ensuring that the isothermal curves are orthogonal to each other. We denote the isothermal curves by $\psi_u(v = \text{constant})$, and $\psi_v(u = \text{constant})$.

Theorem 1. *Given a pair of orthogonal vector fields $(\mathbf{w}_u, \mathbf{w}_v)$ at a point $p \in \mathcal{S}$, where $\frac{d\psi_u}{dt}(0) = \mathbf{w}_u, \frac{d\psi_v}{dt}(0) = \mathbf{w}_v$, and $\psi_u(0) = \psi_v(0) = p$, there always exists a parameterization $\mathbf{x}$ in the neighborhood of p such that the coordinate curves of $\mathbf{x}$ are the integral curves of $\mathbf{w}_u$ and $\mathbf{w}_v$.*

The proof of Theorem 1 due to Korn-Lichtenstein [20, 21] uses the notion of the first fundamental form of surfaces, and the reader is referred to Varolin [22] for a modern proof. The fundamental idea here is that one can always recover a surface patch locally using the vector fields on the isothermal curves. Further, the entire surface can be reconstructed using a collection of such overlapping local patches. We thus represent the surface $\mathcal{S}$ by the coordinate map given by the collection of curves,

$$\Psi \equiv (\{\psi_u\}, \{\psi_v\}), \forall u, v \in [0, 1], \text{where} \tag{2}$$

$$\psi_u, \psi_v : [0, 2\pi] \to \mathbb{R}^3 \Big| \int_0^{2\pi} \dot{\psi}_{u(t)} dt = \int_0^{2\pi} \dot{\psi}_{v(t)} dt = 0. \tag{3}$$

We list a few properties of the set Ψ below.

1. Since Ψ is defined intrinsically on the surface, it is invariant to rigid motions (translations and rotations) of the surface.
2. Any angle-preserving mapping of the original surface generates a new Ψ that will consist of a new family of isothermal curves. The original Ψ can be recovered up to a diffeomorphism of the plane or the sphere.
3. The coordinate map Ψ can alternately be generated as a solution of the Laplace's equation $\Delta f = 0$ for any harmonic function $f : \mathcal{S} \to \mathbb{R}$.

2.1 Construction of Isothermal Curves using Conformal Mapping

Any regular surface admits an isothermal coordinate system [23]. A collection of isothermal coordinate systems under a particular orientation defines a Riemannian structure on the surface. Furthermore, such a surface is locally conformal to a plane. Then the coordinate functions of any two transition or overlapping charts on this surface are holomorphic. We will exploit this idea to construct isothermal curves on surfaces. Particularly, in our work, isothermal curves are computed from a global conformal mapping of the

Fig. 1: Example of coordinate curves on a hippocampal surface.

surface with a holomorphic 1-form based method [24]. As discussed earlier, holomorphic functions and the associated differential forms can be generalized to Riemann surfaces by using the notion of conformal structure. For example, a *holomorphic 1-form* ω is a complex differential form, such that in each local frame, (u_α, v_α), $z_\alpha = u_\alpha + \mathbf{i}v_\alpha$, where $\mathbf{i} = \sqrt{-1}$, the parametric representation is $\omega = f(z_\alpha)dz_\alpha$, where $f(z_\alpha)$ is a holomorphic function. On a different chart $\{U_\beta, \phi_\beta\}$, with another local frame , (u_β, v_β), $z_\beta = u_\beta + \mathbf{i}v_\beta$, where $\mathbf{i} = \sqrt{-1}$, we have $\omega = f_\beta(z_\beta)dz_\beta = f_\beta(z_\beta(z_\alpha))\frac{dz_\beta}{dz_\alpha}dz_\alpha$, where $f_\beta\frac{dz_\beta}{dz_\alpha}$ is still a holomorphic function. By Hodge theory, one may compute holomorphic 1-forms [24] on simply connected (such as the cortex) or multiply connected (such as the hippocampus) surfaces, where the computed holomorphic 1-forms induce a surface
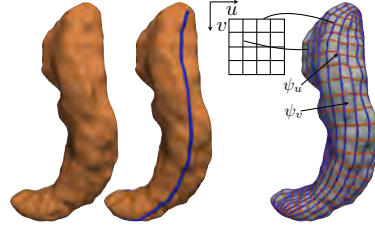
conformal parameterization on the Euclidean domain. For both hippocampal and cortical surfaces, the holomorphic 1-form induces a special system of curves on a surface, the so-called *conformal net*. Horizontal trajectories are the curves that are mapped to iso-v lines in the parameter domain. Similarly, vertical trajectories are the curves that are mapped to iso-u lines in the parameter domain. The horizontal and vertical trajectories form a web on the surface. Because the holomorphic 1-form induces a conformal parameterization, these curves become isothermal curves defined in the prior section. For a tube-like shape or a genus zero surface with one open boundary, the trajectory connectivity structure is trivial (as there is no zero point). Our work uses these trajectories as the curves defined on surface to represent an intrinsic coordinate system. Fig. 1 shows an example of a conformal net on a hippocampal surface.

For some anatomical shapes, we label two consistent landmark curves at the anterior and the posterior end. For example, in case of the hippocampus, we represent its anterior junction with the amygdala, and its posterior limit as it turns into the white matter of the fornix. These are biologically valid and consistent landmarks across subjects. We call this process *topological optimization*. Given the hippocampal tube-like shape, the landmarks curves can be automatically identified by finding the extreme points by searching along the first principal direction of geometric moments of the surface [25]. By cutting along these two landmark curves, a hippocampal surface is modeled by a cylinder-like surface, i.e. a multiply connected surface. Alternately, the cortex is represented by a genus zero surface with one open boundary by cutting along the boundary of the corpus callosum.

3   Elastic Shape Matching between Surfaces

Given two surfaces $\mathcal{S}_1$ and $\mathcal{S}_2$, and their coordinate maps Ψ_1 and Ψ_2, we will find an optimal mapping by deforming the coordinate maps from one surface to the other. Since the map Ψ is not scale invariant, we normalize the scale as follows. First in a neighborhood of a point $p \in \mathcal{S}$, we have the local curve parameterizations $\psi_u : t \in [0, 2\pi) \rightarrow \mathbb{R}^3$, and $\psi_v : t \in [0, 2\pi) \rightarrow \mathbb{R}^3$, that are used to define the local surface parameterization as $\frac{\partial \mathbf{x}}{\partial u} = \frac{d\psi_u}{dt}\frac{dt}{du}, \frac{\partial \mathbf{x}}{\partial v} = \frac{d\psi_v}{dt}\frac{dt}{dv}$. Then the scale normalization is achieved using,

$$\tilde{\Psi} = \frac{\Psi}{\sqrt{\int_{\mathcal{D}} ||\frac{\partial \mathbf{x}}{\partial u} \times \frac{\partial \mathbf{x}}{\partial v}|| du\ dv}} \tag{4}$$

With a slight abuse of notation, we will refer to the scale-normalized map $\tilde{\Psi}$ as Ψ throughout the paper. For rotational alignment, we will first compute the centroids of the set of any one of the coordinate curves. For example, for surface $\mathcal{S}_1$, we compute $\sigma_u^1 = \int_0^1 \psi_u du, \forall u \in [0, 1]$. Here $\sigma_u^1 \in \mathbb{R}^3, \forall u \in [0, 1]$. Similarly, for surface $\mathcal{S}_2$, we compute $\sigma_u^2 = \int_0^1 \psi_u du, \forall u \in [0, 1]$. Then the optimal rotation ($\hat{O} \in SO(3)$) is initialized by carrying out a singular value decomposition $\hat{O} =$

$ADB^T = \int_0^1 \sigma_u^1 \sigma_u^2 du$, where A and B are left and right unitary matrices, and D is a matrix given by

$$D = \begin{bmatrix} 1 & 0 & 0 \\ 0 & 1 & 0 \\ 0 & 0 & |A||B| \end{bmatrix}.$$

(5)

Our approach is as follows. We simultaneously obtain a global as well as a locally optimal matching of the surface via its isothermal curves. Instead of explicitly imposing a Riemannian metric on the underlying geometrical structure, as done in [14, 26], we propose a distance function on the coordinate curves directly. Figure 2 shows the schematic of the workflow.
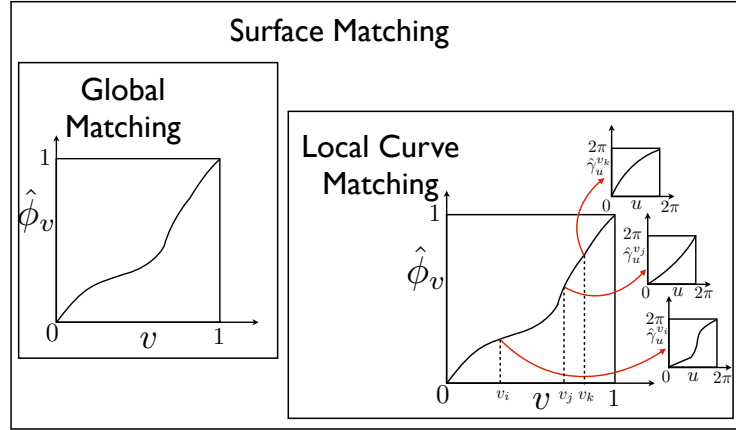

Fig. 2: Illustration of the global and local surface matching procedure. For each $v \in [0, 1]$, there is a local diffeomorphism of the isothermal curve.

3.1 Global Matching between Surfaces

In order to simplify the global matching, we observe that the isothermal curves ψ_v can also be written as functions of u, since ψ_u can be reconstructed from ψ_v owing to orthogonality. We will thus simplify the notation in Eqn. 3 and by slight abuse of notation, denote the surface by the collection,

$$\Psi \equiv \{\psi_v(u)\}, \text{where } u \in [0, 2\pi),$$

(6)

$$\psi_v : [0, 2\pi] \to \mathbb{R}^3 \Big| \int_0^{2\pi} \dot{\psi}_v(u) du = 0, \forall v \in [0, 1].$$

(7)

Let the coordinate maps Ψ_1, and Ψ_2 be given by $\{\psi_v^1(u)\}$, and $\{\psi_v^2(u)\}$ respectively. Then we define the matching problem as the minimizer,

$$d_{\mathcal{S}}(\Psi_1, \Psi_2) = \min_{\phi_v} \int_0^1 d_\psi(\psi_v^1, \hat{O} \, \psi_{\phi_v}^2)^2 [1 + \dot{\phi}_v] dv,$$

(8)

where $\phi_v : [0, 1] \to [0, 1]$ is a diffeomorphism, and $v \in [0, 1]$ is the index of the isothermal curve. Furthermore d_ψ is the distance between isothermal curves v,

and ϕ_v for a given v, and is defined in Sec. 3.2. Ideally, we would like the distance $d_{\mathcal{S}}$ to be inverse-consistent and invariant to reparameterizations by the index of the isothermal curve s.

Proposition 1. *The distance $d_{\mathcal{S}}$ is invariant to reparameterization by the index function of the isothermal curves.*

Proof. In order to check for invariance due to reparameterization, we evaluate Eqn. 8 under an arbitrary reparameterization of the time parameter $\lambda(v)$: $[0,1] \rightarrow [0,1]$. Without loss of generality, we set $\hat{O} = I$, an identity matrix Thus Eqn. 8 becomes

$$d_{\mathcal{S}}(\Psi_1(\lambda(v)), \Psi_2(\lambda(v))) = \operatorname*{argmin}_{\phi_{\lambda(v)}} \int_0^1 d_\psi\big(\psi^1_{\lambda(v)}, \psi^2_{\phi(\lambda(v))}\big)^2 [1 + \dot{\phi}(\lambda(v))]\dot{\lambda}(v)dv.$$

(9)

By performing a change of variables $\lambda(v) = g$, and letting $\lambda(0) = 0, \lambda(1) = 1$ without loss of generality, we get $dg = \dot{\lambda}(v)dv$. Also we note that $\frac{d}{dv}\phi(\lambda(v)) = \dot{\phi}(\lambda(v))\dot{\lambda}(v)dv$. Thus the reparameterized distance becomes

$$\operatorname*{argmin}_{\phi_g} \int_0^1 d_\psi\big(\psi^1_g, \psi^2_{\phi_g}\big)^2 [1 + \dot{\phi}_g]dg,$$

(10)

which is same as Eqn. 8.

Proposition 2. *Given that the distance between the isothermal curves d_ψ is symmetric, then the distance $d_{\mathcal{S}}$ is an inverse-consistent (symmetric) distance between coordinate maps.*

Proof. In order to check for inverse-consistency, we need to verify that $d_{\mathcal{S}}(\Psi_1, \Psi_2)$ under the optimal time warp $\hat{\phi}_v$ is same as $d_{\mathcal{S}}(\Psi_2, \Psi_1)$ under the optimal time warp $\hat{\phi}_v^{-1}$. Again, without loss of generality, we set $\hat{O} = I$, an identity matrix. Noting that $\frac{d}{dv}\phi_v^{-1} = \frac{1}{\dot{\phi}(\phi_v^{-1})}$ under the inverse function theorem, we rewrite Eqn. 8 as

$$d_{\mathcal{S}}(\Psi_2, \Psi_1) = \min_{\phi_v^{-1}} \int_0^1 d_\psi\big(\psi^2_v, \psi^1_{\phi_v^{-1}}\big)^2 \Big[1 + \frac{1}{\dot{\phi}_v(\phi_v^{-1})}\Big]dv.$$

(11)

Again by change of variables we let $\phi_v^{-1} = t$. Thus $dv = \dot{\phi}_v dt$. Therefore the above distance becomes

$$d_{\mathcal{S}}(\Psi_2, \Psi_1) = \min_{\phi_v^{-1}} \int_0^1 d_\psi(\psi^1_v, \psi^2_{\phi_v})^2 [\dot{\phi}(t) + 1]dt,$$

(12)

which is same as Eqn. 8.

3.2   Local Curve Matching of Coordinate Parameterizations

The objective function (Eqn. 8) for global matching involves the curve distance between isothermal curves, and further requires it to be symmetric. To obtain an

efficient, invariant and symmetric mapping between coordinate curves ψ_v^1, and ψ_v^2, we consider the following distance function:

$$d_\psi(\psi_v^1, \psi_v^2) = \underset{r, O \in SO(3), \gamma_u \in \mathbb{S}^1}{\operatorname{argmin}} \frac{1}{2} \int_0^{2\pi} \left[\left\langle \psi_v^1 - r \cdot O(\psi_v^2 \circ \gamma_u), \psi_v^1 - r \cdot O(\psi_v^2 \circ \gamma_u) \right\rangle \right. $$
$$\left. + \left\langle \psi_v^2 - r \cdot O(\psi_v^1 \circ \gamma_u^{-1}), \psi_v^2 - r \cdot O(\psi_v^1 \circ \gamma_u^{-1}) \right\rangle \right] du, \tag{13}$$

where the operation $r \cdot \psi_v^1 = \psi_v^1(s - r)|_{\mathrm{mod}2\pi}$, simply shifts the starting point of the curve, $O \in SO(3)$ is a local rotation, and $\gamma : \mathbb{S}^1 \to \mathbb{S}^1$ is a local reparameterization. For a discretized version of the curve, the shift in origin r is found exhaustively, and the optimal rotation is found using singular value decomposition as described before. Finally, given an optimal shift and rotation, we solve Eqn. 13 using dynamic programming. Eq. 13 is symmetric, which also causes the distance defined in Eq. 8 to be symmetric. It should be noted that the Eq. 8 jointly optimizes the mapping in both u and v directions via the global parameterization ϕ_v in Eqn. 8 and the local parameterization γ_u in Eqn. 13.

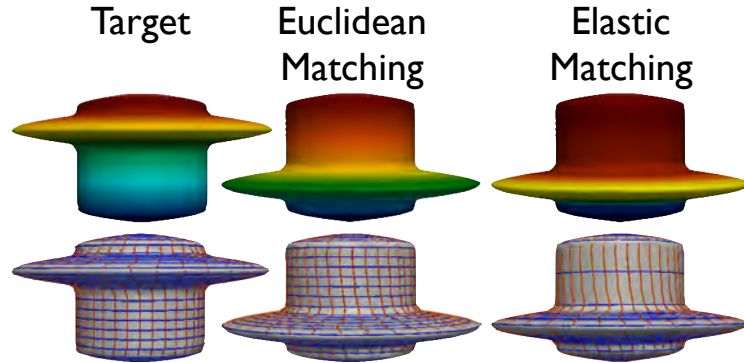## 4   Results

4.1   Synthetic Data

Fig. 3: Comparison of Euclidean and elastic surface matching for synthetic data. Top row shows the matching features in color. Bottom row shows the corresponding parameterizations.

The synthetic data consists of two cylindrical shapes that differ by the locations of the protrusions along the length. We use the same method as the hippocampal surface to induce isothermal curves on them. Although this is a manufactured example, the alignment resulting from shape matching provides insights about the behavior of the algorithm. Fig. 3 (top row) shows the target and the source shapes color coded according to the parameterization in the v direction. The middle column shows the Euclidean matching of the source to the target. This is achieved by setting $\phi_v = id, \forall v \in [0, 1]$, and $\gamma_u = id$ for each v.

The last column shows the elastic shape matching of the source by minimizing Eq. 8 and Eq. 13. The bottom row shows the respective parameterizations resulting from the matching. In the last column, we observe that the optimal matching is achieved by shifting the bump downward, while preserving the features (shown by color) on the bump. Thus the corresponding parameterization (last row, last column) shows large stretching before the bump, and compression immediately after. We also show a smooth deformation between the target to the source for
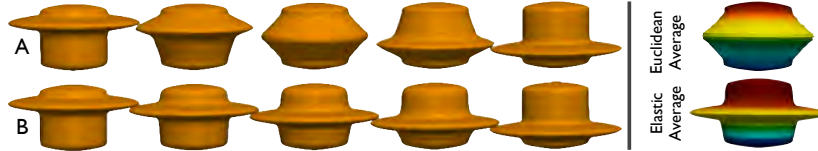

Fig. 4: Left panel: Smooth deformations between the target and the source shapes for A. Euclidean matching, and B. Elastic matching. Right panel: Average shapes using Euclidean and elastic matching.

both Euclidean matching (Fig. 4 A) and the elastic matching (Fig. 4 B). The right panel in Fig. 4 also shows the average shapes. The average shape for the elastic matching preserves the bump as well as the parameterization (shown by color) compared to the Euclidean case.

4.2   Cortical Registration

Here, we show an example of matching intrinsic coordinate maps between two cortical surfaces, extracted using the MNI protocol [27]. Fig. 5 shows comparisons of Euclidean and elastic matching of the coordinate maps for the cortical surfaces. It should be noted that no sulcal curves were traced on the surfaces, and that the shape matching is landmark-free. The circles highlight where there is a noticeable improvement in cortical homology due to the elastic matching. While this example is for demonstration purposes only, and the nature of the cortical correspondence warrants careful validation, our goal here was to illustrate the potential for a simple elastic curve registration based method to solve a general surface matching problem.

4.3   Hippocampal shape analysis

For the purpose of hippocampal morphometry, the imaging data consisted of high resolution T1 MRI images of 40 healthy subjects (15 Males / 25 Females) in the age range $18 - 80$ years with the mean age of 44 ± 20 years. The hippocampal surface meshes were segmented using Freesurfer [28] and the intrinsic coordinate maps were generated using the procedure in Sec. 2.1. Fig. 6 shows the shape alignment between pairs of target and the source hippocampi from this dataset. Each row of Fig. 6 shows the source hippocampus followed by the aligned target due to Euclidean matching, and the aligned target shape due to elastic matching. All shapes are color-coded according to the underlying parameterization, and the structural alignment can be visualized by similar colors. Visually, the elastic
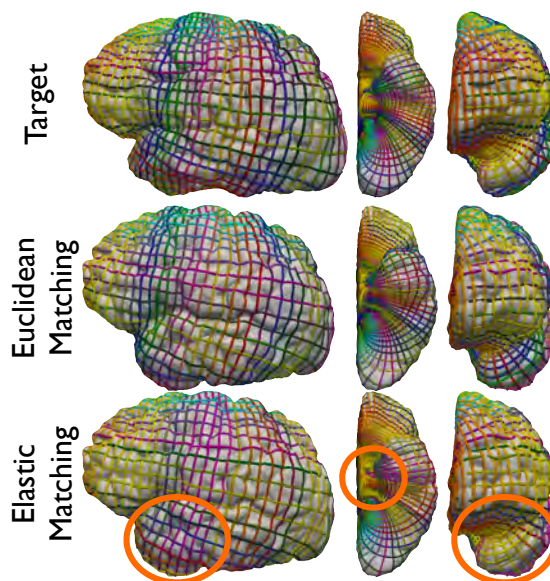
Fig. 5: Cortical surface mapping between the target shape (top) and the source shape using Euclidean (middle) and elastic matching (bottom). Also shown are the coordinate curves colored according to the parameterization. Circles denote improvement in registration due to elastic matching.

matching yields a better alignment as observed in the anterior (top), central, and the posterior regions.

We then performed statistical analysis of the morphology of the hippocampus to model the effect of age on the shape. We selected an arbitrary shape in the dataset as the template and aligned all the surfaces to it using the elastic shape matching. Then all the aligned surfaces were grouped together, and an average shape of the hippocampal surfaces was computed for both the left and the right hemisphere in the brain. Finally for each aligned surface, we computed the radial distance from each vertex on the surface to the medial axis. This distance was used as the shape variable in the statistical analysis. We used a general linear model for inferring the effect of age after covarying for gender on the hippocampal morphology. Fig. 7 shows the statistically significant p-values (after correcting for multiple comparisons using the false discovery rate yielding a cut-off value $p = 0.01$) overlaid on three different views of the averages of the left and the right hippocampus. These shapes were uniformly scaled, so the results show contractions exclusively due to shape with the progression of age. This result is in agreement with the established knowledge that the brain volume and also the hippocampal volume atrophies with age. Finally we also performed supervised classification to determine the accuracy of hippocampal shape as a predictor for age. We defined the two classes as subjects with age ≤ 30 years, and those with age > 30 years. We then computed the distance given in Eqn. 8

Target   Euclidean   Elastic
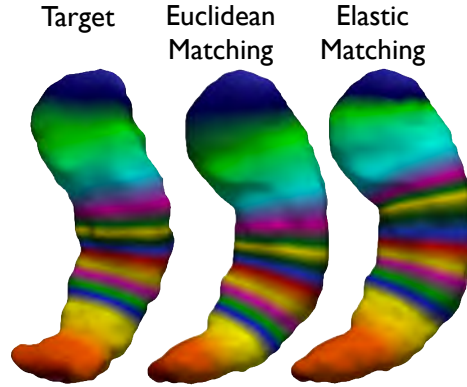   Matching   Matching

Fig. 6: Shape matching for hippocampal surfaces, colored according to the parameterization. Each row shows a different matched pair of hippocampal shapes.

L   R   L   R   L   R

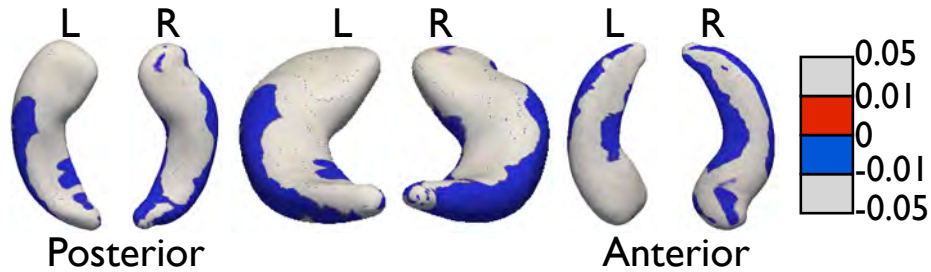Posterior   Anterior

Fig. 7: Significant age effects (corrected for multiple comparisons) on hippocampal shape shown by p-values after applying a general linear model (GLM) covarying for gender. The colormap is shown at the bottom.

between the individual shapes to the mean and used it as a classifier in a support vector machine (SVM) framework. When computing distances, we computed the shape distances in the following ways i) based on exhaustive matching of the conformal nets, and ii) based on partial matching ($\pm$ 20 coordinate curves from the center) of the conformal nets from individuals to the mean shape. Fig. 8 shows the accuracy for predicting the age based on hippocampal shape for the two strategies. We observed that the average accuracy improved from 57.5% to 62.5% when we restricted the matching to the subset of the conformal nets. This may be because the classification of age may be sensitive to morphological changes near the center of the shape (Also see Fig. 7).

5   Discussion

We presented a geometric approach for mapping intrinsic coordinate systems across shapes. The coordinate systems are derived from the holomorphic 1-form that exploits the conformal structure of the surface. Bidirectional coordinate

57.5%	Age < 30	Age > 30
Age < 30	11	8
Age > 30	9	12

62.5%	Age < 30	Age > 30
Age < 30	11	6
Age > 30	9	14

(a)   (b)

Fig. 8: Percent Accuracy and confusion matrix for age prediction from hippocampal shape after training a 10-fold SVM classifier. Percent accuracy differs depending upon (a) Exhaustive matching of conformal nets from individual to mean, and (b) Partial matching of conformal nets from individual to mean.

matching is achieved jointly using both a global diffeomorphic warping function as well as a local diffeomorphic function invariant to local coordinate reparameterizations. This achieves both global shape alignment while optimizing local shape correspondences. In the future, we will investigate methods for performing statistical shape analysis of surfaces via the coordinate map representation, as well as perform detailed validation and comparisons with other approaches such as the spectral methods for subcortical shapes, as well as fluid-based registration approaches for cortical surfaces.

References

1. Piegl, L.: On NURBS: a survey. Computer Graphics and Applications, IEEE **11**(1) (1991) 55–71
2. Reuter, M., Wolter, F.E., Peinecke, N.: Laplace–Beltrami spectra as Shape-DNA of surfaces and solids. Computer-Aided Design **38**(4) (2006) 342–366
3. Qiu, A., Bitouk, D., Miller, M.I.: Smooth functional and structural maps on the neocortex via orthonormal bases of the Laplace-Beltrami operator. IEEE Transactions on Medical Imaging **25**(10) (2006) 1296–1306
4. Reuter, M., Wolter, F.E., Shenton, M., Niethammer, M.: Laplace–Beltrami eigenvalues and topological features of eigenfunctions for statistical shape analysis. Computer-Aided Design **41**(10) (2009) 739–755
5. Shi, Y., Morra, J., Thompson, P., Toga, A.: Inverse-consistent surface mapping with Laplace-Beltrami eigen-features. In: Information Processing in Medical Imaging, Springer (2009) 467–478
6. Styner, M., Oguz, I., Xu, S., Brechbühler, C., Pantazis, D., Levitt, J.J., Shenton, M.E., Gerig, G.: Framework for the statistical shape analysis of brain structures using SPHARM-PDM. The Insight Journal (1071) (2006) 1–20
7. Chung, M.K., Robbins, S.M., Dalton, K.M., Davidson, R.J., Alexander, A.L., Evans, A.C.: Cortical thickness analysis in autism with heat kernel smoothing. NeuroImage **25**(4) (2005) 1256–1265
8. Shen, L., Makedon, F.: Spherical mapping for processing of 3d closed surfaces. Image and Vision Computing **24**(7) (2006) 743–761
9. Joshi, S., Pizer, S., Fletcher, P.T., Yushkevich, P., Thall, A., Marron, J.: Multiscale deformable model segmentation and statistical shape analysis using medial descriptions. IEEE Transactions on Medical Imaging **21**(5) (2002) 538–550

10. Bouix, S., Pruessner, J.C., Louis Collins, D., Siddiqi, K.: Hippocampal shape analysis using medial surfaces. Neuroimage **25**(4) (2005) 1077–1089
11. Pizer, S.M., Fletcher, P.T., Joshi, S., Thall, A., Chen, J.Z., Fridman, Y., Fritsch, D.S., Gash, A.G., Glotzer, J.M., Jiroutek, M.R., et al.: Deformable M-reps for 3D medical image segmentation. International Journal of Computer Vision **55**(2) (2003) 85–106
12. Yushkevich, P.A., Zhang, H., Gee, J.C.: Continuous medial representation for anatomical structures. IEEE Transactions on Med. Imaging **25**(12) (2006) 1547–1564
13. Beg, M.F., Miller, M.I., Trouvé, A., Younes, L.: Computing large deformation metric mappings via geodesic flows of diffeomorphisms. International Journal of Computer Vision **61**(2) (2005) 139–157
14. Kurtek, S., Klassen, E., Ding, Z., Jacobson, S.W., Jacobson, J.L., Avison, M.J., Srivastava, A.: Parameterization-invariant shape comparisons of anatomical surfaces. IEEE Transactions on Med. Imaging **30**(3) (Mar 2011) 849–858
15. Durrleman, S., Pennec, X., Trouvé, A., Ayache, N.: Statistical models of sets of curves and surfaces based on currents. Medical Image Analysis **13**(5) (2009) 793–808
16. Dryden, I., Mardia, K.: Statistical analysis of shape. John Wiley & Son (1998)
17. Cootes, T.F., Taylor, C.J., Cooper, D.H., Graham, J., et al.: Active shape models-their training and application. Computer Vision and Image Understanding **61**(1) (1995) 38–59
18. Auzias, G., Lefevre, J., Le Troter, A., Fisher, C., Perrot, M., Regis, J., Coulon, O.: Model-driven harmonic parameterization of the cortical surface: Hip-hop. IEEE Transactions on Medical Imaging **32**(5) (2013) 873–887
19. Srivastava, A., Samir, C., Joshi, S.H., Daoudi, M.: Elastic shape models for face analysis using curvilinear coordinates. Journal of Mathematical Imaging and Vision **33**(2) (2009) 253–265
20. Osserman, R.: Zwei anwendungen der methode der sukzessiven approximationen. Festschrift fur H.A. Schwarz, Springer (1914) 215–229
21. Lichtenstein, L.: Zur theorie der konformen abbildung: Konforme abbildung nichtanalytischer, singularitätenfreier flächenstücke auf ebene gebiete. Bull. Acad. Sci. Cracovie, Cl. Sci. Math. Nat. Ser. A (1916) 192–217
22. Varolin, D.: Riemann surfaces by way of complex analytic geometry. Volume 125. American Mathematical Soc. (2011)
23. Donaldson, S.K.: Riemann surfaces. Oxford University Press Oxford (2011)
24. Wang, Y., Lui, L.M., Gu, X., Hayashi, K.M., Chan, T.F., Toga, A.W., Thompson, P.M., Yau, S.T.: Brain surface conformal parameterization using Riemann surface structure. IEEE Transactions Med. Imag. **26**(6) (June 2007) 853–865
25. Elad, M., Milanfar, P., Golub, G.H.: Shape from moments-an estimation theory perspective. IEEE Transactions on Signal Processing **52**(7) (2004) 1814–1829
26. Pennec, X.: Left-invariant Riemannian elasticity: a distance on shape diffeomorphisms? In: 1st MICCAI Workshop on Mathematical Foundations of Computational Anatomy: Geometrical, Statistical and Registration Methods for Modeling Biological Shape Variability. (2006) 1–13
27. Holmes, C., MacDonald, D., Sled, J., Toga, A., Evans, A.: Cortical peeling: CSF/grey/white matter boundaries visualized by nesting isosurfaces. Visualization in Biomedical Computing (1996) 99–104
28. Dale, A.M., Fischl, B., Sereno, M.I.: Cortical surface-based analysis. I. segmentation and surface reconstruction. NeuroImage **9**(2) (1999) 179–94